Planetary Gearbox Fault Diagnosis Using a Single Piezoelectric Strain Sensor

Jae Yoon[1], David He[2], Brandon Van Hecke[3], Thomas J. Nostrand[4], Junda Zhu[5], and Eric Bechhoefer[6]

[1,2,3]*University of Illinois at Chicago, Chicago, IL, 60607, USA*
jyoon52@uic.edu
davidhe@uic.edu
bvanhe2@uic.edu

[4,5]*Renewable NRG Systems, Hinesburg, VT, 05461, USA*
tjn@renewablenrgsystems.com
jz@renewablenrgsystems.com

[6]*Green Power Monitoring Systems, Essex Junction, VT, 05452, USA*
eric@gpms-vt.com

ABSTRACT

Planetary gearboxes are widely used in the drivetrain of helicopters and wind turbines. Any planetary gearbox failure could lead to breakdown of the whole drivetrain and major loss of helicopters and wind turbines. Therefore, planetary gearbox fault diagnosis is an important topic in prognostics and health management (PHM). Planetary gearbox fault diagnosis has been done mostly through vibration analysis over the past years. Vibration signals theoretically have the amplitude modulation effect caused by time variant vibration transfer paths due to the rotation of planet carrier and sun gear, and therefore their spectral structure is complex. It is difficult to diagnose planetary gearbox faults via vibration analysis. Strain sensor signals on the other hand have less amplitude modulation effect. Thus, it is potentially easy and effective to diagnose planetary gearbox faults via stain sensor signal analysis. In this paper, a research investigation on planetary gearbox fault diagnosis via strain sensor signal analysis is reported. The investigation involves using time synchronous average technique to process signals acquired from a single piezoelectric strain sensor mounted on the housing of a planetary gearbox and extracting condition indicators for fault diagnosis. The reported investigation includes analysis results on a set of seeded fault tests performed on a planetary gearbox test rig in a laboratory. The results have showed a satisfactory planetary gearbox fault diagnostic performance using strain sensor signal analysis.

1. INTRODUCTION

Gearboxes are widely used in almost every powertrain of rotating systems such as automobile, helicopter, wind turbine, and etc. According to Link *et al.* (2011), approximately 59% of the failure modes in wind turbines involved gear failures. Astridge *et al.* (1989) indicated that 19.1% of all the helicopter transmission failures came from the gear failure. Gearbox failures are normally accompanied by unexpected increment in operation cost and catastrophic disaster followed by loss of life. Especially, the planetary gearbox (PGB) is one of the most critical components in generating uplift force in a helicopter transmission system and converting wind power to electrical power in a wind turbine drive train system. However, the fault detection of planetary gearbox is very complicate since the complex nature of dynamic rolling structure of planetary gearbox does not allow for direct attachment of sensors within the rotating elements. A large portion of planetary gearbox diagnostic system has been devoted to vibration analysis using accelerometers. A vibration analysis technique namely "vibration separation" was introduced by McFadden & Howard (1990), Howard (1990), and McFadden (1991). Vibration separation enables to decompose a raw vibration signal into multiple PGB component (*e.g.* sun, planet, or ring) oriented vibration signals by taking windowed vibration signals only when the vibration sensor, ring gear, planet gear, and sun gear are aligned inline. The windowed vibration signals are recombined specifically for the targeted gear component by utilizing the geometric properties of corresponding PGB. Subsequent studies by McFadden (1994), Samuel *et al.* (2004), and Lewicki *et al.* (2011) validated this research with slightly modified versions of the technique. However, the fundamental idea of vibration separation remains unchanged. Wu *et al*. (2004) have shown the detectability of planet carrier crack in a planetary gearbox. In their study, raw vibration data and time synchronous average (TSA) data were transferred to frequency domain and wavelet domain to obtain differentiable features. In a paper by Patrick *et al*. (2007), a vibration data based framework for on-board fault diagnosis and failure prognosis of helicopter transmission component was presented. In their study, TSA pre-processed vibration data and particle filter based diagnostic and prognostic models were presented. Yu *et al*. (2010) compared a raw vibration signal and TSA signal with a wavelet transformed vibration signal to obtain desirable fault feature. Bartelmus & Zimroz (2009) showed that the spectral characteristics of vibration signal obtained from planetary gear help not only fault detection but also gear fault location. Feng & Zuo (2012) derived mathematical models of faulty planetary gear for detecting and locating fault by considering characteristic frequency of amplitude modulation (AM) and frequency modulation (FM) effects.

In a recent paper, Feng & Zuo (2013) pointed out that vibration signals theoretically have the amplitude modulation effect caused by time variant vibration transfer paths due to the unique dynamic structure of rotating planet gears. Therefore, it is difficult to diagnose PGB faults via vibration analysis. One attractive solution to this problem is to use alternative sensor signals that have less sensitivity to AM effect for PGB fault diagnosis and prognosis. Feng & Zuo (2013) have shown the effectiveness of torsional vibration analysis for PGB fault diagnosis using a torque sensor. The frequency characteristics of torsional vibration were shown to be solely sensitive to the AM and FM effects caused by gear faults under constant torque on input and output shafts. Kiddy *et al.* (2011) used fiber optic strain signals for PGB fault diagnosis and showed a close relationship between strain measurement and torque changes. Even though promising, the research reported in the literature on using less AM effect sensitive signals for PGB fault diagnosis has certain limitations. The torque sensors used by Feng and Zuo (2013) are more expensive than vibration and strain sensors and require special installation. The fiber optic strain sensor array used by Kiddy *et al*. (2011) had to be embedded in the PGB in order to be effective. The strain signals of fiber optic strain sensor can only be sampled at a maximum sampling rate up to 1 kHz, which limits its coverage on shaft speed above 2060 rpm. Also in Kiddy *et al*. (2011), the strain signals were analyzed the same way as vibration signals. Fiber optic sensor signals were analyzed using vibration separation technique after low frequency components were filtered out. No effective signal analysis techniques have been developed for strain signals. Piezoelectric (PE) strain sensor is desirable in having an improved strain resolution and applicability of higher sampling rate in comparison with the conventional strain gauge sensors (Banaszak 2001) or the fiber optic strain sensors (Jiang *et al.* 2014).

To overcome the above mentioned challenges in developing effective PGB fault diagnosis capability, a research investigation on planetary gearbox fault diagnosis via strain sensor signal analysis has been conducted and is reported in this paper. The PE strain sensors based planetary gearbox fault diagnosis method can be considered as an attractive alternative to traditional vibration analysis based approaches. A key characteristic of PE materials is the utilization of the direct piezoelectric effect to sense structural deformation and the converse piezoelectric effect to actuate structures. Compared to the conventional strain gauge sensors and accelerometers, the PE strain sensors have certain advantages that could be summarized as follows: (1) ability to measure the first derivative of physical deformation with less sensitive AM and FM effect , (2) high linearity and sensitivity from their superior noise immunity as compared to differentiated sensing performance of conventional strain sensors (Lee & O'Sullivan, 1991, Banaszak 2001), (3) high frequency range (Jiang *et al.* 2014), (4) space-efficiency without a structural change on the measuring target (Kon *et al*. 2007), and (5) negligible high temperature effect on the measurement output (Sirohi & Chopra, 2000, Jiang *et al.* 2014). The aforementioned benefits allow for PE strain sensors to potentially have greater sensing resolution and accuracy.

The remainder of the paper is organized as follows. Section 2 gives a detailed explanation of the proposed methodology. In Section 3, the details of the seeded fault tests on a laboratory planetary gearbox test rig and the experimental setup used to validate the proposed methodology are provided. Section 4 presents the planetary gearbox fault diagnosis results from the seeded fault tests. Finally, Section 5 concludes the paper.

2. METHODOLOGY

An overview of the proposed methodology is provided in Figure 1. First, the PE strain sensor signals and tachometer signals are digitized simultaneously. Then, a band pass filter is applied so that the band passed signals could contain the information related to the planetary gearbox conditions. Using the tachometer signals, the TSA signals can be obtained along with residual signal and energy operator (EO). Residual signal is the TSA signal with shaft and mesh frequencies being removed and EO is a type of residual of the autocorrelation function (Teager, 1992).

In a related research on rotating machinery diagnostics, it has been shown that a deliberately chosen band pass filter improves diagnostic performance by removing shaft imbalance (Shiroishi *et al*., 1997). Thus, a band pass filter with low frequency bandwidth (*i.e.,* low pass filter) was applied to get the information associated with the gearbox condition while high frequency noises could be removed.

The major components of the methodology are explained in the following two sections. Section 2.1 provides a brief review of TSA and the computation of condition indicators (CIs) used for planetary gearbox fault diagnosis is explained in Section 2.2.

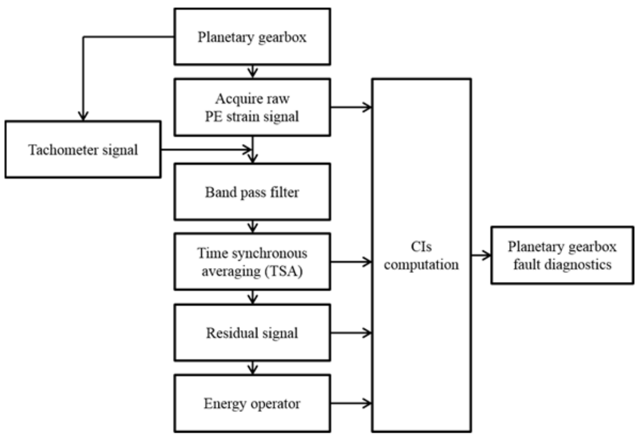

Figure 1. Overview of the methodology.

2.1. Time Synchronous Average

TSA is one of the most widely utilized signal processing techniques to extract a periodic waveform from noisy signals of rotating machines. The underlying idea of TSA is to obtain a periodically repeated waveform of interest over N number of revolutions. Theoretically, when a rotating machine is running at a constant speed, the periodic waveform is intensified while any noises are suppressed with a noise reduction rate of $\frac{1}{\sqrt{N}}$.

Consider a signal $x(t)$ composed of a periodic signal $y(t)$ with known period T_R and additive noise $e(t)$:

$$x(t) = y(t) + e(t) \tag{1}$$

Assuming the total number of N observed periods, the TSA of $x(t)$ can be expressed as:

$$a(t) = \frac{1}{N}\sum_{r=0}^{N-1} x(t - rT_R) \tag{2}$$

As $N \to \infty$, the TSA signal $a(t)$ approaches to $y(t)$. More details about TSA could be found in (Braun, 1975; McFadden, 1987; Bechhoefer and Kingsley, 2009).

Basically, TSA chops up the raw sensor signal into multiple single revolution signals. Then, each revolution signals are resampled (via stretching or shrinking) so as to have same sample points in one revolution. Then, the final periodic signal is obtained by averaging the resampled signals. After TSA is computed, any kind of fault detection condition indicators can be evaluated. Two major types of TSA techniques have been reported in the literature: TSA with tachometer as a reference signal and tachometer-less TSA. Since comparing those two techniques is beyond the scope of this paper, only the TSA with tachometer will be addressed herein. Even though successful TSA applications to many types of signals such as vibration and acoustic emission (AE) signals have been reported in the literature (Mcfadden, 1987; Bonnardot *et al*., 2005; and Qu *et al*., 2014), application of TSA to PE strain signal processing for planetary gear fault diagnosis has not yet been reported.

2.2. CIs for Planetary Gearbox Fault Diagnosis

Table 1 provides the definitions of the CIs investigated for PGB fault diagnosis. The CIs can be defined into five general types: root mean square (*RMS*), peak to peak (*P2P*), skewness (*SK*), kurtosis (*KT*), and crest factor (*CF*). Each type of CI can be computed using different input signals. In addition to TSA signals, other types of input signals can be generated: residual, narrow band (NB), AM, and FM. Residual is a TSA signal with the primary meshing and shaft components removed. The energy operator (EO) introduced by Teager (1992) is defined as the residual of the autocorrelation function as following:

$$x_{EO,i} = x_i^2 - x_{i-1}\cdot x_{i+1}, \quad (\text{for } i = 2, 3, \ldots, N-1) \tag{3}$$

where $x_{EO,i}$ is the i^{th} element of EO data; x_i is the i^{th} element of the input data x_{IN}. NB signals could be obtained by applying a narrow band pass filter on the TSA data. The width of the narrow band can be selected based on the gear fault frequency. In this paper, three narrow bands are selected based on sun gear fault frequency, planet gear fault frequency, and ring gear fault frequency, respectively. Finally, AM and FM signals are obtained by amplitude modulation and phase modulation of the narrow band filtered data.

3. EXPERIMENTAL SETUP

This section covers the experimental setup used to validate the PE strain sensor based planetary gearbox fault diagnostic technique. Figure 2 displays the planetary gearbox test rig used to collect the PE strain sensor data under different gear health and operating conditions.

3.1. The Planetary Gearbox Test Rig

The planetary gearbox test rig composes four main parts: (1) the data acquisition (DAQ) system, (2) the driving motor, (3) the gearbox, (4) the load generator. The DAQ system includes a National Instruments' DAQ board with a maximum analog input sampling rate of 1.25 MHz, a PE strain sensor, and a signal conditioner from PCB Piezotronics. The driving motor is a 3-phase 10HP induction motor with a motor controller. A Hall effect sensor was used as the tachometer paired with a toothed

Table 1. The definitions of the CIs.

CI	Description / Equation	Input Signal (x_{IN}): TSA	Residual	EO	NB	AM	FM
		Time synchronous averaged signal (x_{TSA})	TSA signal with the primary meshing and shaft components removed (x_{Res})	Energy operator: a residual of the autocorrelation function (x_{EO})	Narrow band pass filtered (x_{NB})	Amplitude modulation of NB filtered signal ($AM(x_{NB})$)	Frequency modulation of NB filtered signal ($FM(x_{NB})$)
Root mean square (RMS)	$RMS(x_{IN}) = \sqrt{\frac{1}{N}\sum_{i=1}^{N} x_i^2}$	$RMS(x_{IN})$: measures the magnitude of a discretized signal.					
Peak to peak ($P2P$)	$P2P(x_{IN}) = \frac{(\max_{1\le i\le N}(x_i) - \min_{1\le i\le N}(x_i))}{2}$	$P2P(x_{IN})$: measures the maximum difference within the data range.					
Skewness (SK)	$SK(x_{IN}) = \frac{\frac{1}{N}\sum_{i=1}^{N}(x_i-\bar{x})^3}{\left[\sqrt{\frac{1}{N}\sum_{i=1}^{N}(x_i-\bar{x})^2}\right]^3}$	$SK(x_{IN})$: measures the asymmetry of the data about its mean value. A negative SK value and positive SK value imply the data has a longer or fatter left tail and the data has a longer or fatter right tail, respectively.					
Kurtosis (KT)	$KT(x_{IN}) = \frac{N\sum_{i=1}^{N}(x_i-\bar{x})^4}{\left[\sum_{i=1}^{N}(x_i-\bar{x})^2\right]^2}$	$KT(x_{IN})$: measures the peakedness, smoothness, and the heaviness of tail in a data set.					
Crest factor (CF)	$CF(x_{IN}) = \frac{P2P(x_{IN})}{RMS(x_{IN})}$	$CF(x_{IN})$: measures the ratio between $P2P(x_{IN})$ and $RMS(x_{IN})$ to describe how extreme the peaks are in a waveform.					

Note: x_i is i^{th} element of the input data x_{IN}; N is the length of the input data x_{IN}; max(·) returns the maximal element of input data x_{IN}; min(·) returns the minimal element of input data x_{IN}; $\bar{x}$ is a mean value of the input data x_{IN} defined as $\sum_{i=1}^{N} x_i / N$; NB, AM, and FM refers to a narrow band, amplitude modulation, and frequency modulation, respectively.

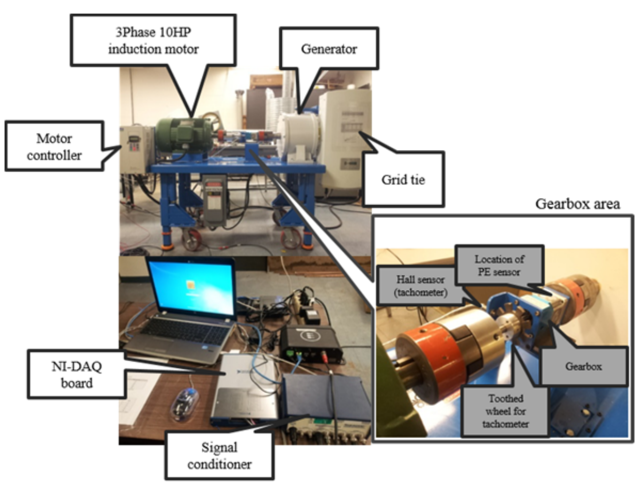

Figure 2. The planetary gearbox test rig for wind turbine simulator.

wheel mounted on the motor shaft. The output shaft of the gearbox is connected to a generator and a grid tie to serve as a load generator. The structure of the PGB test rig is similar to those used in a wind turbine. In this study, a commercially available single stage planetary gearbox with a 5:1 speed reduction ratio was used. In Figure 3, a notional sketch of the planetary gearbox structure is provided. Amongst the three different planetary gearbox types, a specific planetary gearbox with standstill ring gear was used in this paper. For this type PGB, the number of teeth is linear to the radius of each gears pitch circle. This indicates that the gear ratio is also related to the angular velocity (ω) of the gears. The gear ratio can be defined as:

$$R = \frac{\omega_1}{\omega_A} = 1 + \frac{z_3}{z_1} \quad (4)$$

where ω_i is the angular velocity of the i^{th} gear component; z_i is the number of teeth on the i^{th} gear component; the gear component index subscripts 1, 2, 3, and A correspond to sun gear, planet gear, ring gear, and arm (*i.e.* planet carrier), respectively. The planet carrier rotation speed (*i.e.* output shaft speed) in frequency could be obtained as:

$$f_a = \frac{f_1}{R} \tag{5}$$

where f_i is the rotation speed in frequency at the i^{th} gear component. Also, a meshing characteristic frequency of planetary gearbox can be obtained as:

$$f_{12} = f_{23} = \frac{f_1 z_1 z_3}{(z_1 + z_3)} = \frac{f_1 \cdot z_3}{R} \tag{6}$$

where f_{ij} is the relative rotation speed in frequency between the i^{th} and j^{th} gear component.

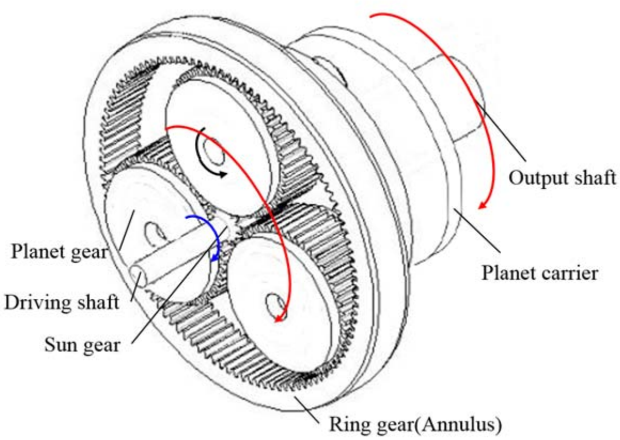

Figure 3. Notional sketch of the planet gearbox structure.

The most common three failure modes of a planetary gearbox are: sun gear fault, planet gear fault, and ring gear fault. Their corresponding fault frequencies are represented as follows:

$$f_{f,1} = s \cdot (f_1 - f_a) = \frac{f_1 z_3 s}{(z_1 + z_3)} \tag{7}$$

$$f_{f,2} = 2(f_2 + f_a) = \frac{4 n_1 z_1 z_3}{(z_3^2 - z_1^2)} \tag{8}$$

$$f_{f,3} = s \cdot f_a = \frac{f_1 z_1 s}{(z_1 + z_3)} \tag{9}$$

where $f_{f,i}$ represents the fault frequency at the i^{th} gear component; s represents the number of planet gears in the gearbox. For more details, see (Bartelmus and Zimroz, 2011). Tables 2 and 3 present the structural information and characteristic frequencies of the planetary gearbox used in this study.

Table 2. The parameters of the planetary gearbox

Parameter	Number of teeth on sun gear (z_1)	Number of teeth on planet gear (z_2)	Number of teeth on ring gear (z_3)	Number of planet gears (s)
Value	27	41	108	3

Table 3. Characteristic frequencies of the planetary gearbox at varied input shaft speed.

Input shaft speed (f_1)	Output shaft speed (f_a)	Meshing frequency ($f_{12} = f_{23}$)	Sun gear fault frequency ($f_{f,1}$)	Planet gear fault frequency ($f_{f,2}$)	Ring gear fault frequency ($f_{f,3}$)
10	2	216	24	10.67	6
20	4	432	48	21.33	12
30	6	648	72	32	18
40	8	864	96	42.67	24
50	10	1080	120	53.33	30

* All the values are in unit of Hz.

3.2. Seed Gear Faults

Three types of planetary gearbox faults were created: sun gear tooth fault, planet gear tooth fault, and ring gear tooth fault. Each type of the gear fault was created by artificially damaging a tooth on a sun gear, planetary gear, and rig gear, respectively (see Figure 4).

During the seeded fault tests, PE strain signals were collected with a sampling rate of 100 kHz. The tachometer signals were simultaneously recorded along with the PE strain signals to get revolution stamps. Both the healthy gearbox and the gearboxes with seeded faults were tested at 5 different input shaft speeds: 10 Hz, 20 Hz, 30 Hz, 40 Hz, and 50 Hz. At each speed, five samples were collected. In addition to the shaft speed variation, varying loading conditions were applied at the output shaft of the gearbox: 0%, 25%, 50%, and 75% of the maximum torque of the planetary gearbox. At each loading condition, 25 samples (five samples per shaft speed for 5 speeds) were taken. In addition, the PE strain sensors were mounted at the same location of the gearbox for each data collection.

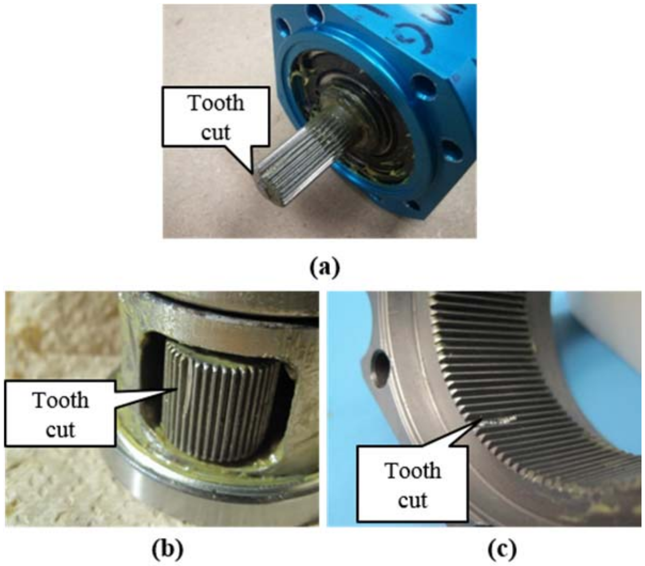

Figure 4. Seeded faults: (a) sun gear fault, (b) planet gear fault, (c) ring gear fault.

4. RESULTS

The validation results for the seeded fault tests conducted on the planetary gearbox test rig are provided in this section. Figure 5 shows a sample of the PE strain sensor signal and tachometer signal at 10Hz shaft speed for a duration of 0.3 seconds. Since the toothed wheel associated with the tachometer in the test rig has eight teeth, each input shaft revolution results in 8 zero crossings.

Before the TSA was computed, a band pass filter with a bandwidth of 1 Hz to 18 kHz was applied to the signals.

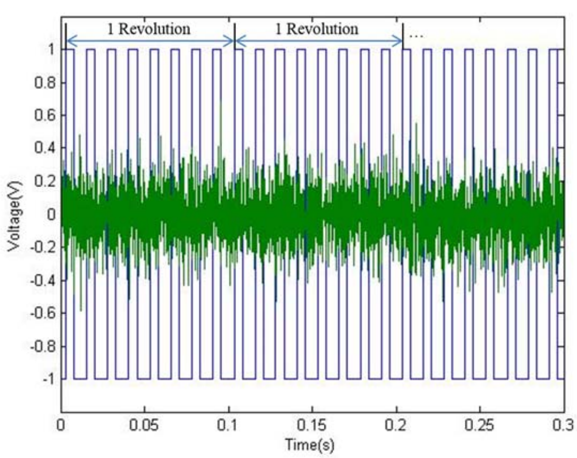

Figure 5. Sample of the healthy PE strain sensor signal and tachometer signal at 10Hz shaft speed.

Samples of the TSA signals of the PE strain sensor are provided in Figures 6 through 8. Figure 6 shows the TSA samples of the healthy gearbox with 50% loading at different shaft speeds. Figure 7 shows TSA samples with a shaft speed of 30Hz at different loading conditions. In Figure 8, TSA samples for different gearbox health conditions with shaft speed fixed at 30 Hz and loading at 50% are provided.

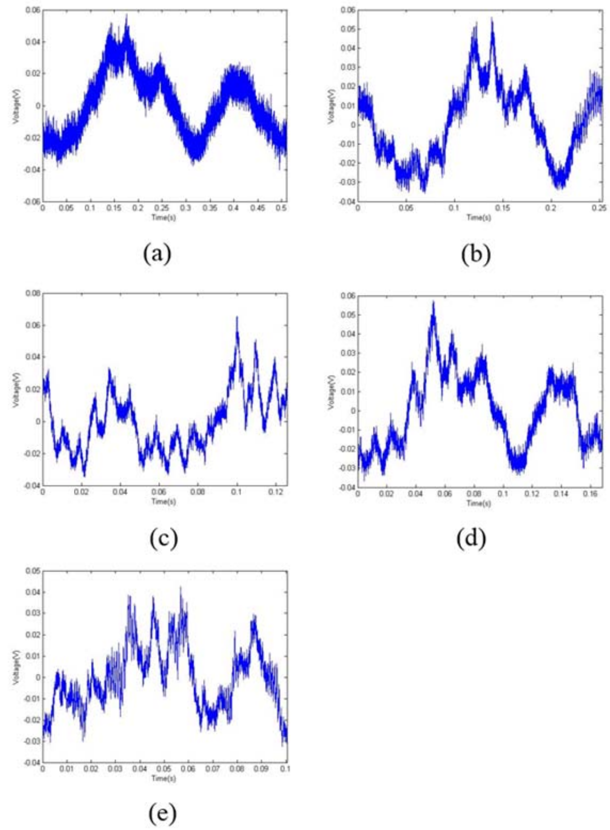

Figure 6. Samples of PE strain sensor signals of the healthy gearbox at different shaft speeds: (a) 10 Hz, (b) 20 Hz, (c) 30 Hz, (d) 40 Hz, (e) 50 Hz.

Once the TSA signals were obtained, then all of the CIs described in Section 2.4 were computed. Among the computed CIs, four of them were found effective: TSA RMS, TSA P2P, residual RMS, and residual P2P.

Figure 9 shows the TSA RMS plots for different gearbox health conditions at different shaft speeds and loading conditions. As one can see from Figure 9, by using TSA RMS alone, the three gear faults can be clearly separated. As the loading increases, the separation of the gear faults gets better. Also, by using TSA RMS alone, all the three gear faults can be clearly separated from the healthy condition. The detectability of the gear faults gets better as the loading increases. For all the 4 gearbox conditions, noted from Figure 9, the TSA RMS remains relatively stationary within the same loading condition regardless the change of the shaft speed. This shows that the PGB gear fault diagnostic capability of the TSA RMS is heavily affected by the torque level of the gearbox. The vertical bar for each data point shown in Figure 9 represents a 95% confidence interval of the estimated TSA RMS mean. In order to check the statistical significance of the gear fault separation using TSA RMS, analysis of variance (ANOVA) test was conducted using the TSA RMS data. In this test, it was assumed that the shaft speed has no effect on TSA RMS within a loading condition.

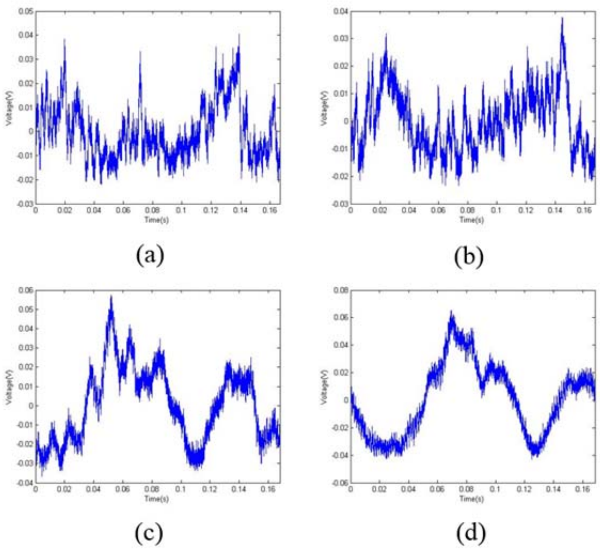

Figure 7. Samples of the PE strain sensor signals at different loading conditions: (a) 0%, (b) 25%, (c) 50%, (d) 75%.

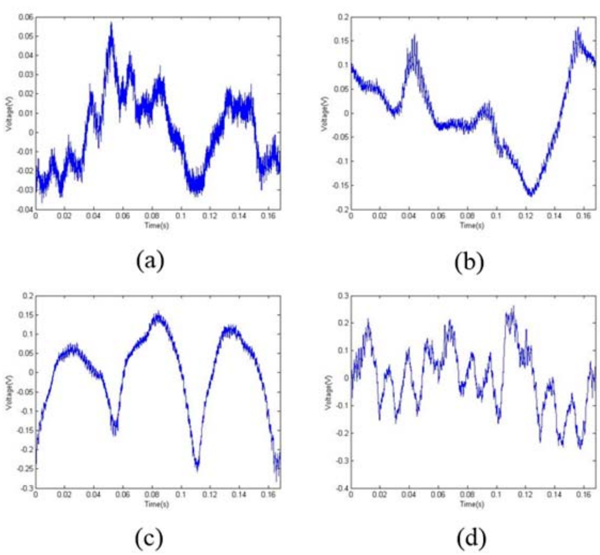

Figure 8. Samples of the PE strain sensor signals of different gearbox conditions: (a) healthy gearbox, (b) sun gear fault, (c) planet gear fault, (d) ring gear fault.

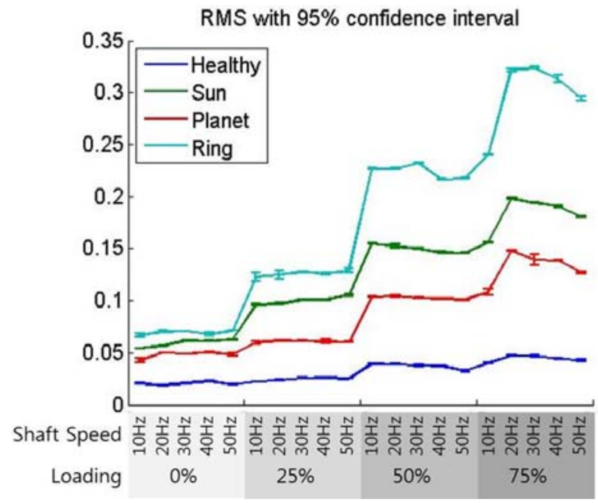

Figure 9. TSA RMS plots .

The following hypotheses were established based on aforementioned assumptions:

$$\mathrm{H}_0: \mu_1 = \mu_2 = \mu_3 = \mu_4$$
$$\mathrm{H}_1: \text{at least one } \mu_i \neq \mu_j \quad (10)$$
$$(\text{for } i, j = 1,2,3, \text{and } 4;\ i \neq j)$$

where μ_i is mean TSA RMS of the i^{th} gear health condition at a fixed loading condition, i = 1, 2, 3, and 4 represents healthy gearbox, sun gear fault, planet gear fault, and ring gear fault, respectively. Table 4 shows the summary of ANOVA results with a 99% confidence level.

From Table 4, *P*-values for all loading conditions are 0.000. With a 99% confidence level, the null hypotheses should be rejected ($\alpha = 0.01 > 0$). Therefore, it is safe to say that the separation of all the gear faults tested using TSA RMS is statistically significant at all loading conditions.

Table 4. Summary of ANOVA results for TSA RMS.

Loading	Source	DF	SS	MS	*F*	*P*
0%	Factor	3	0.0334141	0.0111380	1605.12	0.000
	Error	96	0.0006662	0.0000069		
	Total	99	0.0340802			
25%	Factor	3	0.1481272	0.0493757	8261.04	0.000
	Error	96	0.0005738	0.0000060		
	Total	99	0.1487010			
50%	Factor	3	0.4641124	0.1547041	10614.42	0.000
	Error	96	0.0013992	0.0000146		
	Total	99	0.4655116			
75%	Factor	3	0.845794	0.281931	781.55	0.000
	Error	96	0.034630	0.000361		
	Total	99	0.880424			

The results for other three CIs: TSA P2P, residual RMS, and residual P2P are presented in the same way as TSA RMS in the following. The resulting plots of the CIs are provided in Figures 10 to 12 and the ANOVA results in Tables 5 to 7, respectively.

Similar results like TSA RMS can be observed for other two CIs: TSA P2P and residual RMS. However, the diagnostic performance of these two CIs at 0% loading condition is not as good as TSA RMS. A clear diagnosis of the gear faults can be observed at 25%, 50%, and 75% loading conditions. When the loading level reaches 25% or above, TSA P2P and residual RMS can be ranked like TSA RMS as the following order: ring gear fault -> planet gear fault -> sun gear fault -> healthy gear. For residual P2P, a clear diagnosis of the gear faults can be observed only when the loading level reaches to 50% or above.

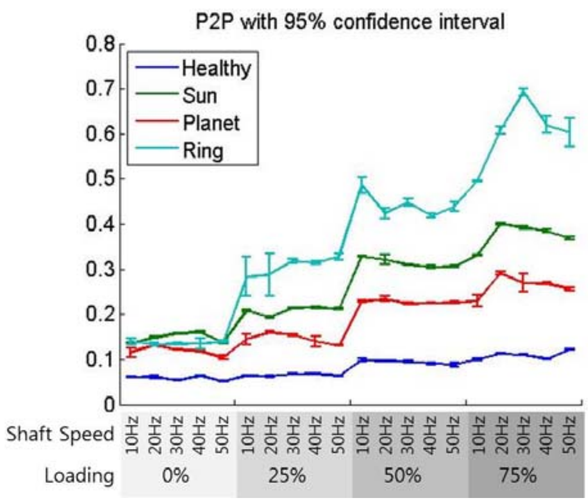

Figure 10. TSA P2P plots.

Table 5. Summary of ANOVA results for TSA P2P.

Loading	Source	DF	SS	MS	*F*	*P*
0%	Factor	3	0.1199638	0.0399879	611.06	0.000
	Error	96	0.0062822	0.0000654		
	Total	99	0.1262461			
25%	Factor	3	0.775791	0.258597	1065.47	0.000
	Error	96	0.023300	0.000243		
	Total	99	0.799091			
50%	Factor	3	1.615071	0.538357	2682.91	0.000
	Error	96	0.019264	0.000201		
	Total	99	1.634335			
75%	Factor	3	3.25105	1.08368	787.88	0.000
	Error	96	0.13204	0.00138		
	Total	99	3.38309			

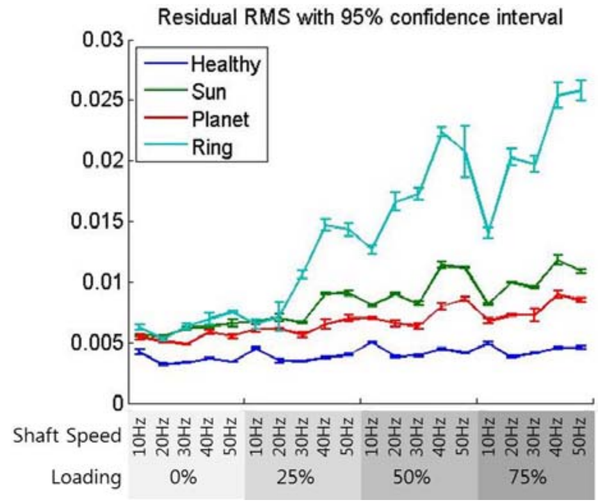

Figure 11. Residual RMS plots.

Table 6. Summary of ANOVA results for residual RMS.

Loading	Source	DF	SS	MS	*F*	*P*
0%	Factor	3	0.0001227	0.0000409	147.50	0.000
	Error	96	0.0000266	0.0000003		
	Total	99	0.0001493			
25%	Factor	3	0.0006061	0.0002020	56.46	0.000
	Error	96	0.0003436	0.0000036		
	Total	99	0.0009497			
50%	Factor	3	0.0025676	0.0008559	219.08	0.000
	Error	96	0.0003750	0.0000039		
	Total	99	0.0029427			
75%	Factor	3	0.0038871	0.0012957	233.04	0.000
	Error	96	0.0005337	0.0000056		
	Total	99	0.0044208			

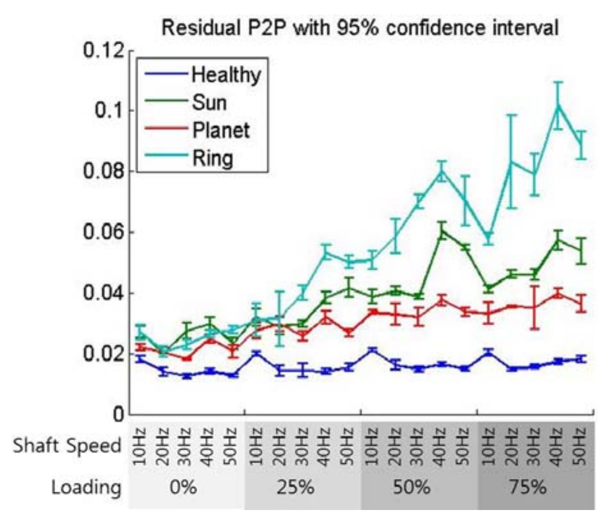

Figure 12. Residual P2P plots.

Table 7. Summary of ANOVA results for residual P2P.

Loading	Source	DF	SS	MS	*F*	*P*
0%	Factor	3	0.0019954	0.0006651	76.63	0.000
	Error	96	0.0008333	0.0000087		
	Total	99	0.0028287			
25%	Factor	3	0.0087545	0.0029182	79.85	0.000
	Error	96	0.0035084	0.0000365		
	Total	99	0.0122630			
50%	Factor	3	0.0323371	0.0107790	193.51	0.000
	Error	96	0.0053475	0.0000557		
	Total	99	0.0376846			
75%	Factor	3	0.0557005	0.0185668	239.39	0.000
	Error	96	0.0074456	0.0000776		
	Total	99	0.0631462			

Note that in Tables 5 to 7, even under the low loading conditions, the null hypothesis in (10) is rejected. This is because all the faulty CIs are significantly different from the healthy CIs even though the difference among the faulty CIs is not statistically significant.

5. CONCLUSIONS

In this paper, a new piezoelectric strain sensor based planetary gearbox fault diagnostic methodology was presented. The presented method was accomplished through a combination of band pass filtering, time synchronous average, and condition indicators to extract diagnostic features for planetary gear box diagnosis. First, the PE strain sensor signal is band pass filtered so as to retain the information related to the gear conditions. Then, TSA signal is computed to obtain the periodically repeated waveform while white noise is suppressed. The presented method was validated using data collected from seeded fault tests conducted on a planetary gearbox test rig in a laboratory. The validation results have shown that, by utilizing the TSA based PE strain sensor signal processing approach, fully separable diagnostic CIs towards all planetary gearbox fault types were captured regardless of shaft speed and output shaft loading condition. The current planetary gearbox diagnostic methods mainly rely on vibration signal analysis. They provide limited fault diagnosis for planetary gearboxes. The PE strain sensor based diagnostic technique presented provides an attractive alternative to the current vibration analysis based approach.

REFERENCES

Astridge, D. G. (1989). Helicopter transmissions - design for safety and reliability, *Proceedings of Mechanical Engineers: Journal of Aerospace Engineering*, Vol. 203, No. 2, pp. 123 - 138.

Bartelmus, W., & Zimroz, R. (2009). Vibration condition monitoring of planetary gearbox under varying external load, *Mechanical Systems and Signal Processing*, Vol. 23, No. 1, pp. 246 - 257.

Bartelmus, W., & Zimroz, R. (2011). Vibration spectra characteristic frequencies for condition monitoring of mining machinery compound and complex gearboxes, *Scientific Papers of the Institute of Mining, University of Technology, Studies and Research*, Vol. 133, No 40, pp. 17 - 34.

Banaszak, D. (2001). Comparison of piezoelectric strain sensors with strain gages, *Proceedings of the Annual Meeting of the American Statistical Association*, Atlanta, GA, Aug 5 – 9.

Bechhoefer, E. & Kingsley, M. (2009). A review of time synchronous average algorithm, *Annual Conference of the Prognostics and Health Management Society, Sep 27 – Oct 1*, San Diego, CA.

Bonnardot, F., Badaoui, M. E., Randall, R. B, Daniere, J., & Guillet, F. (2005). Use of the acceleration signal of a gearbox in order to perform angular resampling (with limited speed fluctuation), *Mechanical Systems and Signal Processing*, Vol. 19, No. pp. 766 - 785.

Braun, S. (1975). The extraction of periodic waveforms by time domain averaging, *Acustica*, Vol. 32, No. 1, pp. 69 - 77.

Feng, Z., & Zuo, M. J. (2012). Vibration signal models for fault diagnosis of planetary gearbox, *Journal of Sound and Vibration*, Vol. 331, No. 22, pp. 4919 – 4939.

Feng, Z. & Zuo, M. J. (2013). Fault diagnosis of planetary gearboxes via torsional vibration signal analysis, *Mechanical Systems and Signal Processing*, Vol. 36, No.2, pp. 401 - 421.

Howard, I. M. (1990). Epicyclic transmission fault detection by vibration analysis, *Australian Vibration and Noise Conference: Vibration and Noise - Measurement, Prediction, and Control*, Melbourne, Australia, pp. 171 - 178.

Jiang, X., Kim, K., Zhang, S., Johnson, J., & Salazar, G. (2014). High-temperature piezoelectic sensing, *Sensors*, Vol. 14, No. 1, pp.144 – 169.

Kiddy, J. S., Samuel, P. D., Lewicki, D. G., LaBerge, K. E., Ehinger, R. T., & Fetty, J. (2011). Fiber optic strain sensor for planetary gear diagnostics, *NASA Technical Report: NASA/TM-2011-217123*, NASA Glenn Research Center, Cleveland, OH.

Kon, S., Oldham, K., & Horowitz, R. (2007). Piezoresistive and piezoelectric MEMS strain sensors for vibration detection, *Proceedings of the SPIE: Sensors and Smart Structures Technologies for Civil, Mechanical, and Aerospace Systems*, Vol. 6529, pp. 1 - 11.

Lee, C. K. & O'Sullivan, T. (1991), Piezoelectric strain rate gages, *Journal of the Acoustical Society of America*, Vol. 90, No.2, pp. 945 - 953.

Lewicki, D. G., Laberge, K. E., Ehinger, R. T., & Fetty, J. (2011). Planetary gearbox fault detection using vibration separation technique, *NASA Technical Report:*

NASA/CR-2004-213068, NASA Glenn Research Center, Cleveland, OH.

Link, H., LaCava, W., van Dam, J., McNiff, B., Sheng, S., Wallen, R., McDade, M., & Lambert, S. (2011). Gearbox reliability collaborative project report: findings from phase 1 and phase 2 testing," *NREL Technical Report: NREL/TP-5000-51885*, National Renewable Energy Laboratory, Golden, CO, USA.

McFadden, P. D. (1987). A revised model for the extraction of periodic waveforms by time domain averaging, *Mechanical Systems and Signal Processing*, Vol. 1, No. 1, pp. 83 - 95.

McFadden, P. D., & Howard, I. M. (1990). The detection of seeded faults in an epicyclic gearbox by signal averaging of the vibration, *Aeronautical Research Laboratory*, Melbourne, Victoria, Australia.

McFadden, P. D. (1991). A technique for calculating the time domain averages of the vibration of the individual planet gears and the sun gear in an epicyclic gearbox, *Journal of Sound and Vibration*, Vol. 144, No. 1, pp. 163 - 172.

McFadden, P. D. (1994). Window functions for the calculation of the time domain averages of the vibration of the individual planet gears and sun gear in an epicyclic gearbox, *Journal of Vibration and Acoustics*, Vol. 116, No. 2, pp. 179 - 187.

Patrick, R., Orchard, M. E., Zhang, B., & Koelemay, M. D. (2007). An integrated approach to helicopter planetary gear fault diagnosis and failure prognosis, *Proceedings of IEEE AUTOTESTCON*, Baltimore, MD, pp. 547 - 552.

Qu, Y., He, D., Yoon, J., VanHecke, B., & Bechhoefer, E. (2014). Gearbox tooth cut fault diagnostics using acoustic emission and vibration sensors - a comparative study, *Sensors*, Vol. 14, No. 1, pp. 1372 - 1393.

Samuel, P. D., Conroy, J. K., & Pines, D. J. (2004). Planetary transmission diagnostics, *NASA Technical Report: NASA/CR-2004-213068*, NASA Glenn Research Center, Cleveland, OH.

Shiroishi, J., Li, Y. Liang, S., Kurfess, T., & Danyluk, S. (1997). Bearing condition diagnosis via vibration and acoustic emission measurement, *Mechanical Systems and Signal Processing*, Vol. 11, No. 5, pp. 693 - 705.

Sirohi, J. & Chopra, I. (2000). Fundamental understanding of piezoelectric strain sensors, *Journal of Intelligent Material Systems and Structures*, Vol. 11, No. 4, pp. 246 - 257.

Teager, H. M., & Teager S. M. (1992). Evidence for nonlinear sound production mechanisms in the vocal tract, in *Speech Production and Speech Modeling Symposium, Time Frequency and Time-Scale Analysis*, edited by Hardcastle, W. J. & Marchal, A., Springer, Netherlands, Vol. 55, pp. 345 - 348, 1992.

Yu, J., Yip, L., & Makis, V. (2010). Wavelet analysis with time-synchronous averaging of planetary gearbox vibration data for fault detection, diagnostics, and condition based maintenance, *2nd International Conference on Mechanical and Electronics Engineering (ICMEE)*, Kyoto, Japan, Vol. 1, pp. 132 - 136.

Wu, B., Saxena, A., Khawaja, T. S., Patrick, R., Vachtsevanos, G., & Sparis, P. (2004). An approach to fault diagnosis of helicopter planetary gears, *Proceedings of IEEE AUTOTESTCON*, San Antonio, TX., pp. 475 - 481.

BIOGRAPHIES

Jae Yoon received his B.E degree in Control engineering from Kwangwoon University, Republic of Korea, worked at Samsung Electronics Co. Ltd. as a product engineer from 2006 through 2008. He then received M.S. degree in Mechanical engineering from the University of Florida. He joined the Intelligent Systems Modeling & Development Laboratory in the department of Mechanical and Industrial Engineering at the University of Illinois-Chicago to pursue Ph.D. degree. His current research interests include: machinery health monitoring for CBM, data-driven methods for diagnostics, and model based and data mining based prognostics, encompassing reliability engineering.

David He Dr. He is a Professor and Director of the Intelligent Systems Modeling & Development Laboratory in the Department of Mechanical and Industrial Engineering at The University of Illinois-Chicago. Dr. He's research areas include: machinery health monitoring, diagnosis and prognosis, complex systems failure analysis, quality and reliability engineering, and manufacturing systems design, modeling, scheduling and planning.

Brandon Van Hecke received his B.S. in Industrial Engineering from the University of Illinois at Chicago in 2010. He is a Ph.D. candidate in the Department of Mechanical and Industrial Engineering. His research interests include digital signal processing, machinery health monitoring, bearing and gear fault diagnostics based on the evaluation of vibration and acoustic emission signals, and condition based maintenance.